Molecular Cancer Therapeutics

MK-4101, a Potent Inhibitor of the Hedgehog Pathway, Is Highly Active against Medulloblastoma and Basal Cell Carcinoma

Gessica Filocamo[1], Mirko Brunetti[1], Fabrizio Colaceci[2], Romina Sasso[2], Mirella Tanori[3], Emanuela Pasquali[3], Romina Alfonsi[4], Mariateresa Mancuso[3], Anna Saran[3], Armin Lahm[5], Lucia Di Marcotullio[4], Christian Steinkühler[1,6], and Simonetta Pazzaglia[3]

Abstract

Aberrant activation of the Hedgehog (Hh) signaling pathway is implicated in the pathogenesis of many cancers, including medulloblastoma and basal cell carcinoma (BCC). In this study, using neonatally irradiated *Ptch1*$^{+/-}$ mice as a model of Hh-dependent tumors, we investigated the *in vivo* effects of MK-4101, a novel SMO antagonist, for the treatment of medulloblastoma and BCC. Results clearly demonstrated a robust antitumor activity of MK-4101, achieved through the inhibition of proliferation and induction of extensive apoptosis in tumor cells. Of note, beside antitumor activity on transplanted tumors, MK-4101 was highly efficacious against primary medulloblastoma and BCC developing in the cerebellum and skin of *Ptch1*$^{+/-}$ mice. By identifying the changes induced by MK-4101 in gene expression profiles in tumors, we also elucidated the mechanism of action of this novel, orally administrable compound. MK-4101 targets the Hh pathway in tumor cells, showing the maximum inhibitory effect on *Gli1*. MK-4101 also induced deregulation of cell cycle and block of DNA replication in tumors. Members of the IGF and Wnt signaling pathways were among the most highly deregulated genes by MK-4101, suggesting that the interplay among Hh, IGF, and Wnt is crucial in Hh-dependent tumorigenesis. Altogether, the results of this preclinical study support a therapeutic opportunity for MK-4101 in the treatment of Hh-driven cancers, also providing useful information for combination therapy with drugs targeting pathways cooperating with Hh oncogenic activity.
Mol Cancer Ther; 15(6); 1177–89.

Introduction

The Hh signal transduction pathway plays a critical role in cell differentiation and patterning during development in many organs/systems. In mammals, the binding of the ligand to its receptor Patched (Ptch1) unleashes Smoothened (SMO) activity. This is followed by inactivation of Suppressor of Fused (SuFu), a negative regulator of the pathway, leading to an intracellular signaling transduction cascade that culminates in GLI-dependent transcriptional activities. Inappropriate activation of the pathway can result in tumorigenesis (1). Germline mutations of the *Ptch1* gene, leading to constitutive Hh signaling, cause Gorlin syndrome, a familial cancer syndrome characterized by neoplasms such as BCC and medulloblastoma (2). Constitutive Hh signaling due to loss-of-function mutations of the *Ptch1* gene (2–5) and less often mutation of *Smo* (6) occurs in the majority of BCCs and in approximately 30% of sporadic medulloblastoma cases (7, 8). Persistent activation of Hh pathway has also been implicated in the pathogenesis of other sporadic human cancer with about 25% of all cancer deaths estimated to involve aberrant Hh activation (9).

Several proteins in the Hh pathway fit into protein families considered pharmacologically tractable and represents possibilities for developing targeted inhibitors. SMO, a G-protein–coupled receptor-like protein, is the most successful target, with numerous antagonists and agonists identified through biochemical and cell-based screening methods. *Ptch1*$^{+/-}$ heterozygous knockout mice (10, 11), the mouse model for Gorlin syndrome, have been critical for development and testing of SMO antagonists (12, 13), several of which have now entered clinical testing (14–16). The most advanced inhibitors of the Hh pathway are the SMO antagonists vismodegib (Curis/Genentech; refs. 17, 18) and LDE225 (Novartis; refs. 19, 20). This study was aimed at investigating the effects of a novel SMO antagonist, MK-4101, for treatment of Hh-driven tumors *in vivo* in *Ptch1*$^{+/-}$ mice (21–23). Irradiation of neonatal *Ptch1*$^{+/-}$ mice increases the frequencies of microscopically detectable preneoplastic stages and full-blown tumors in skin and brain, making these mice an ideal model to test chemotherapy/chemoprevention against Hh-driven tumors *in vivo* (24). Our data demonstrate a robust antitumor activity of MK-4101 *in vivo*, and elucidate its mechanism of action

[1]Exiris, Rome, Italy. [2]IRBM Science Park, Pomezia, Rome, Italy. [3]Laboratory of Biomedical Technologies, Agenzia Nazionale per le Nuove Tecnologie, l'Energia e lo Sviluppo Economico Sostenibile (ENEA) CR-Casaccia, Rome, Italy. [4]Department of Molecular Medicine, University La Sapienza, Rome, Italy. [5]Independent expert, Rome, Italy. [6]Italfarmaco, Cinisello Balsamo, Milan, Italy.

Note: Supplementary data for this article are available at Molecular Cancer Therapeutics Online (http://mct.aacrjournals.org/).

Corresponding Authors: Gessica Filocamo, Exiris s.r.l. Via Savona 6, Rome 00182, Italy. Phone: 390-6702-9882; Fax: 3906-7030-5411; E-mail: gessica_filocamo@exiris.it; and Simonetta Pazzaglia, Laboratory of Radiation Biology and Biomedicine, Agenzia Nazionale per le Nuove Tecnologie, l'Energia e lo Sviluppo Economico Sostenibile (ENEA) CR-Casaccia, Rome, Italy. Phone: 3906-3048-6535; Fax: 3906-3048-3644; E-mail: simonetta.pazzaglia@enea.it

doi: 10.1158/1535-7163.MCT-15-0371

through the identification of MK-4101–driven changes in tumor expression profiles. These findings suggest that MK-4101 is an appealing candidate for treatment of Hh-driven tumors and may have potential therapeutic implications for tumors depending on Hh activity in stromal cells for tumor growth.

Materials and Methods

Mice and irradiation

Mouse model and irradiation conditions were the same as previously described in ref. (21).

Compound and treatments

MK-4101 [$C_{24}H_{24}F_5N_5O$] was designed and synthesized at Merck Sharp and Dohme Laboratories (Supplementary Fig. S1). The compound was dissolved in DMSO for the *in vitro* assays, while for *in vivo* studies it was formulated in 0.5% methylcellulose in deionized water. For pharmacokinetic studies, the compound was administered to C57bl/6 mice or Sprague-Dawley rats. Blood samples ($n = 3$) were collected up to 24 hours postdose and harvested plasma samples were analyzed by LC/MS-MS.

Cell culture and transfection

Embryonic kidney (HEK293T) cells were maintained in DMEM supplemented with 10% FBS, 2 mmol/L L-glutamine, 25 U/mL penicillin, and 25 μg/mL streptomycin. HEK293T cells were purchased from the ATCC in 2010; they were routinely monitored in our laboratory for cellular morphology and microbial presence by microscopic observation and for absence of mycoplasma. No authentication was performed by the authors. Cells were transiently transfected with DreamFectTM Gold reagent (Oz Biosciences).

Bodipy-Cyclopamine binding assay

Mouse Flag-tagged *Smo* WT or *Smo* mutant (D477G) transfected cells were fixed with 4% paraformaldehyde for 10 minutes and incubated for 3 hours at 37°C with Bodipy-Cyclopamine (BC; 5 nmol/L) and test compound, washed with PBS, and permeabilized with TritonX-100 for Hoechst 33258 staining. Fluorescence signals were analyzed in 3–4 representative fields/coverslip (1,000 cells/field) and expressed as percentages of the fluorescence observed in vehicle-treated cells; IC_{50} values were computed by fitting the experimental data with a two-parameter logistic equation using a KaleidaGraph 3.5 software.

Establishment of medulloblastoma/BCC allografts and *in vivo* efficacy studies

Medulloblastoma and BCC tumors derived from *Ptch1*$^{+/-}$ mice were serially passaged subcutaneously *in vivo*. For the efficacy studies, tumors were explanted and single-cell suspensions injected subcutaneously (2.5×10^6 cells/mouse) with 50% Matrigel (BD Biosciences) in 5-week-old CD1 nude female mice (Charles River Laboratories). When tumors reached the average volume required, mice were randomized and treated with MK-4101 orally at doses of 40 or 80 mg/kg once a day, 80 mg/kg twice a day, or with vehicle. Tumor volumes were measured twice a week with a Digimatic Caliper (Mitutoyo); body weight and clinical signs were monitored twice a week.

Histologic analysis and tumor quantification

At the end of treatments, or earlier if sign of illness appeared, *Ptch1*$^{+/-}$ mice were euthanized and autopsied, body and brain weights determined, and brains, skin and skin tumors fixed in 4% buffered formalin. Samples were embedded in paraffin wax, sectioned, and stained with hematoxylin and eosin. The average number of microscopic BCC-like tumors per cm of skin was determined by analyzing the dorsal skin surface (5 cm average length) from *Ptch1*$^{+/-}$ mice ($n = 23$). Cross-sectional areas were taken by measuring the greatest perpendicular diameters through the tumor. Histologic evaluation of brain and skin sections was blinded to the treatment group.

Immunohistochemical analysis

Immunohistochemical analysis of cytokeratin-14 (Covance), Ki-67 (Novocastra), and cleaved caspase-3 (Cell Signaling Technology Inc.) was carried out on 4-μm thick paraffin sections as described previously (22). Digital images were collected by IAS image-processing software (Delta Sistemi) and positive cells counted. Rates of proliferation and apoptosis were calculated as the percentage of positively stained cells relative to the total cell number.

Real-time PCR analysis

Explanted tumors were collected in RNAlater solution (Qiagen) and total RNA was extracted with RNAeasy Mini Kit (Qiagen). Quantitative reverse transcription-PCR (qRT-PCR) of *Gli1* and *Gapdh* mRNA was performed in triplicate by using the Onestep RT-PCR Master Mix and probe sets from Applied Biosystems, in a ABI PRISM 700HT instrument. Quantitative calculations were performed by using the ΔC_t method.

Flow cytometry

Medulloblastoma or BCC cells were cultured at a concentration of 150,000/mL in low adhesion dishes, and treated with 10 μmol/L of MK-4101 for 60 or 72 hours. Newly synthesized DNA was labeled for 4 hours with 10 μmol/L of EdU reagent (ClickIT EdU, Invitrogen) and then detected by addition of the Alexa Fluor 647 azide and CellCycle 405-blue dye.

Western blot analysis

Tumor samples were homogenized in NaCl 150 mmol/L, Tris-Cl pH7.5 20 mmol/L, EDTA 2 mmol/L, EGTA 2 mmol/L, PMSF 0.4 mmol/L, EDTA-free Complete, with a Mixer Mill-MM300 homogenizer (Retsch) at 30 Hz 40″, then lysed in 1% SDS, electrophoresed, and blotted onto a nitrocellulose membrane. Primary antibodies: cyclin B (Santa Cruz Biotechnology); cyclin D1 (Abcam); anti-GAPDH (Abcam); anti-α-tubulin (Sigma).

Microarray experiments

Allograft medulloblastoma tumors ($n = 6$) were randomized in groups and collected at 1, 6, 12, 24, and 36 hours after a single dose or at 24 and 36 hours after the first of two doses of MK-4101 or vehicle. RNAs from explanted tumors were extracted with RNeasy Mini Kit (Qiagen), assayed for quality (Agilent Bioanalyzer) and yield (Ribogreen). Genome scale expression analysis was performed using custom Affymetrix microarrays containing oligonucleotide probes corresponding to 43,682 mouse transcripts/genes (Supplementary Table S1). Sample amplification, labeling, and microarray processing were performed by the Rosetta Inpharmatics Gene Expression Laboratory in Seattle, WA.

Table 1. Efficacy of MK-4101 in several *in vitro* assays

Assay	MK-4101 IC_{50} ± SEM (μmol/L)
*Gli*_luc assay in mouse Light II cells	1.5 ± 0.2
Binding to human recombinant SMO in 293 stable clone	1.1 ± 0.1
In vitro proliferation of *Ptch1*$^{+/-}$ medulloblastoma cells	0.3 ± 0.07
Gli1 mRNA expression in human Kyse180 cells	1.2[a]

Abbreviation: IC_{50}, concentration required for 50% target inhibition.
[a]Average from two independent experiments.

Data were analyzed as described in Supplementary Methods. Microarray data are available at GEO under Accession number GSE77042.

Statistical analysis

All results were presented as mean ± SE. Statistical analysis was performed with the GraphPad Prism software. P values < 0.05 were considered statistically significant.

Results

Identification of MK-4101 as a SMO-binding inhibitor

MK-4101 was originally identified in the 11β-Hydroxy steroid dehydrogenase-1 inhibitor program, from an observation of birth defects induced by this compound in exploratory teratogenicity studies. The malformations observed (holoprosencephaly, cyclopia) were reminiscent of the embryonal toxicity caused by cyclopamine, a natural SMO antagonist, and of the defects elicited by mutations of the Hh pathway. It was subsequently shown that MK-4101 inhibited Hh signaling both in a reporter gene assay in an engineered mouse cell line (*Gli*_Luc) with IC_{50} = 1.5 μmol/L (Table 1; ref. 25), and in human KYSE180 esophageal cancer cells with an IC_{50} = 1 μmol/L. Furthermore, MK-4101 displaced a fluorescently labeled cyclopamine derivative from 293 cells expressing recombinant human SMO with an IC_{50} = 1.1 μmol/L, implying that the compound binds to SMO. MK-4101 also inhibited the proliferation of medulloblastoma cells derived from neonatally irradiated *Ptch1*$^{-/+}$ mice *in vitro* with an IC_{50} = 0.3 μmol/L (25). This inhibition was quantitatively rescued by a SMO agonist, SAG, demonstrating the specificity of its antiproliferative activity. A structurally related compound that however was devoid of any measurable teratogenic effects *in vivo* scored negative in all of these assays (data not shown). Pharmacokinetics of MK-4101 showed that it could be administered orally, showing a good bioavailability (F ≥ 87 %) with low-to-moderate plasma clearance in mice and rats (Table 2). Moreover, it was well absorbed, and mainly excreted into the bile. MK-4101 was not a PgP substrate and mouse brain pharmacokinetics showed significant CNS exposures with a brain AUC/plasma AUC ratio of 0.6. This finding suggests that MK-4101 can be used to treat Hh-dependent brain tumors, such as medulloblastoma.

Table 2. Pharmacokinetics of MK-4101 in different species

Parameter	Mouse	Rat
Dose i.v./p.o. (mg/kg)	1/2	0.5/1
PO nAUC (μmol/L*hour)	3.3	7.4
Cl_p (mL/min/kg)	10	4
V_d (L/kg)	2.5	1.4
$t_{1/2}$ (hours)	2.9	5.9
C_{max} (μmol/L)	1.3	1.2
T_{max} (h)	1	1.5
F_{oral} (%)	97	87

Abbreviations: Cl_p, total plasma clearance; V_d, volume of distribution.

Table 3. Binding of MK-4101 versus vismodegib to wild-type (WT) or mutant (D477G) SMO in transiently transfected 293 cells, expressed as IC_{50} (μmol/L)

Compound	SMO WT	SMO D477G	Folds shift
MK-4101	0.5	7.5	15
Vismodegib	0.011	1.14	100

Clinical data obtained with vismodegib in medulloblastoma (18) or BCC (26) patients suggest that mutations in *Smo* are a dominant mechanism of resistance to this agent. Reasoning that MK-4101 is structurally dissimilar from vismodegib and other SMO antagonists and might interact differently with mutated SMO, we tested MK-4101 for its ability to bind vismodegib-resistant SMO mutated at position D477 (27). While vismodegib showed a 100-fold loss of affinity for the resistant D477G mutant in binding assays, MK-4101 only showed a 15-fold decrease in affinity (Table 3), suggesting MK-4101 as a potential therapeutic agent for vismodegib or sonidegib resistant tumors (28).

As mentioned, MK-4101 is a potent inhibitor of 11β-hydroxy steroid dehydrogenase-1, whose function is the reduction of cortisone to cortisol. Chronic inhibition of this enzyme may affect the hypothalamic–pituitary–adrenal (HPA) axis, by releasing the feedback inhibition exerted by cortisol, possibly leading to altered stress response or adrenal androgen production and hirsutism in women. However, structural analogues of MK-4101 were tested clinically for the treatment of metabolic syndrome and only moderate effects on the production of adrenal androgens (DEHA, androstenedione, and free testosterone) were observed (data not shown). The interesting mutant profile and the excellent drug-like properties of MK-4101 prompted us to set off for a more detailed characterization.

MK-4101 is an efficacious and safe inhibitor of medulloblastoma tumors

To test the efficacy and tolerability of this new compound, we derived allografts in nude mice from medulloblastoma developed in *Ptch1*$^{+/-}$ mice (ref. 21; Fig. 1A). When tumors reached an average volume of 170 mm^3, mice were randomized in groups (n = 10) and treated for 3.5 weeks with 40 or 80 mg/kg of MK-4101 once a day, with 80 mg/kg twice a day, or with vehicle only. None of these regimens significantly decreased body weight or caused other clinically relevant side effects, although a reduction of weight gain might occur at 80 mg/kg twice a day (Fig. 1B). Importantly, MK-4101 showed tumor growth inhibition (40 and 80 mg/kg once a day) and tumor regression at the highest dose (80 mg/kg twice a day; Fig. 1C). Tumors explanted from mice treated with MK-4101 for 24 hours with 40 or 80 mg/kg once a day or with 80 mg/kg twice a day showed a dose-dependent downregulation of *Gli1* mRNA that paralleled the dose-dependent inhibition of tumor growth (Fig. 1D). This finding implies that inhibition of medulloblastoma growth by MK-4101 occurred through targeting of the Hh signaling pathway. The maximum effect for both tumor inhibition and Hh pathway downregulation was achieved at 80 mg/kg twice a day. To better evaluate the potential clinical relevance of MK-4101, we performed a head-to-head comparison versus vismodegib, a "first in class" SMO antagonist. In our allograft model, MK-4101 (80 mg/kg twice a day; n = 10) and vismodegib (50 mg/kg once a day; n = 10) displayed identical antitumor efficacy (Fig. 1E). Moreover, the two compounds also

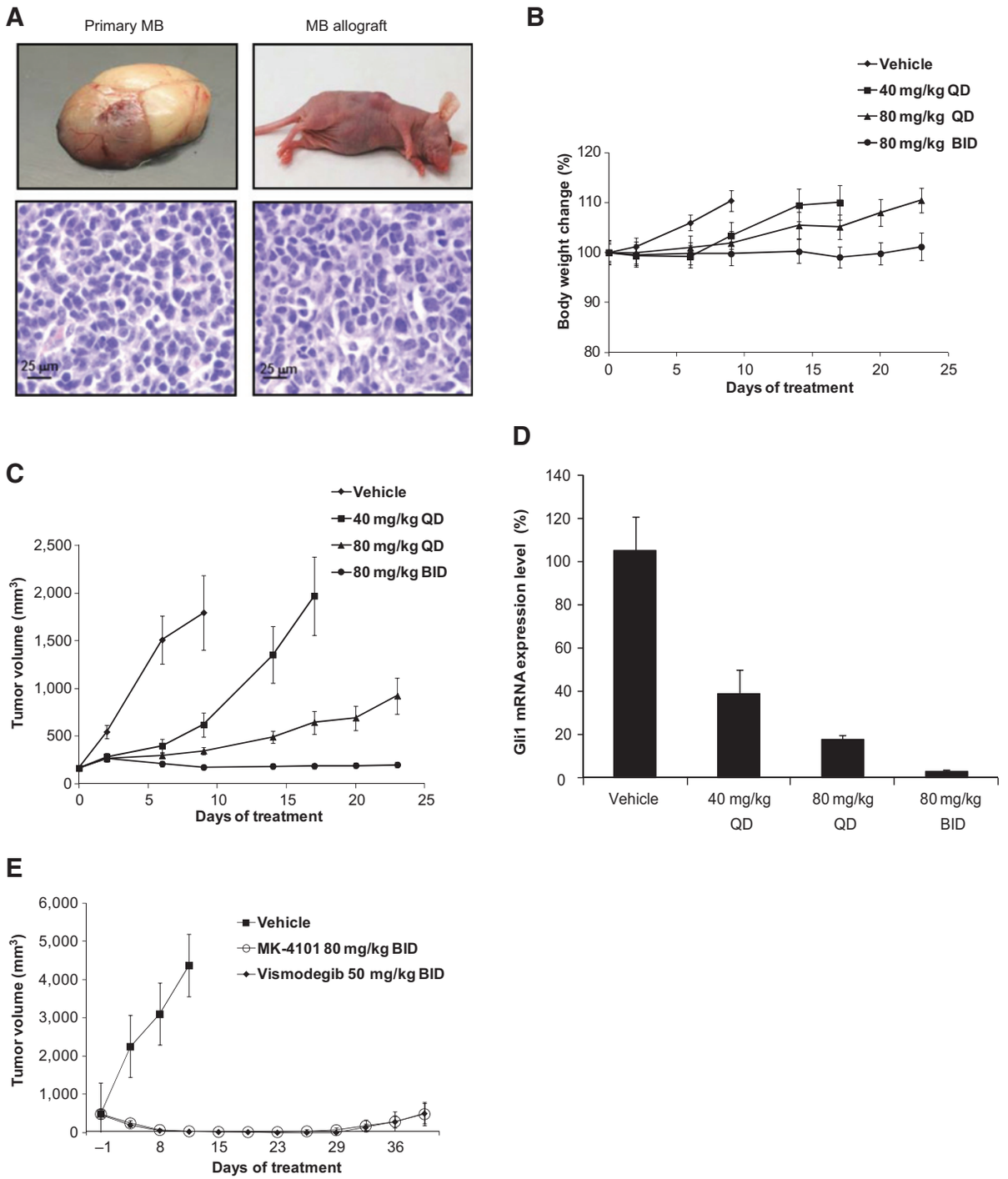

Figure 1.
Determination of optimal dose regimen in transplanted medulloblastoma (MB). A, primary medulloblastoma from *Ptch1*$^{+/-}$ mice and derived allograft whose histology resembles the tumor of origin. B, percentage change in body weight ($n = 10$ ±SE). C, tumor growth inhibition. D, downregulation of tumor *Gli1* mRNA by MK-4101 at 24 hours, after one (QD; once a day) or two (BID; twice a day) doses ($n = 6$ ±SE). E, comparison of preclinical efficacy of MK-4101 and vismodegib on *Ptch1*$^{+/-}$ medulloblastoma allografts ($n = 10$± SE).

showed similar effects on pharmacokinetics/pharmacodynamics (PK/PD; $n = 6$) with comparable downregulation of Gli1 mRNA (Table 4).

MK-4101 treatment eliminates medulloblastoma

We next investigated the effect of MK-4101 on tumor growth at longer term. Mice with medulloblastoma allografts (200 mm^3)

Table 4. Pharmacokinetic/pharmacodynamic profile of MK-4101 versus vismodegib in CD1 female nude mice

		Plasma exposure		Tumor exposure		Residual Gli1 mRNA	
Dose (80 mg/kg)	Time (h)	[μmol/L]	SD	[μmol/L]	SD	% vs. vehicle	SD
MK-4101	6	11.5	1.6	15.7	2.8	13.45	2.20
MK-4101	12	2.4	0.6	3.2	0.9	11.55	3.06
Vismodegib	6	9.4	6.1	6.1	3.9	9.16	2.41
Vismodegib	12	5.6	1.8	4.1	1.6	5.17	4.31

were treated with 80 mg/kg of MK-4101 twice a day ($n = 8$) or vehicle ($n = 8$) for 35 days and afterward tumor growth was monitored for additional 3 months. MK-4101 completely inhibited tumor growth and prevented tumor relapse after treatment termination, strongly suggesting that the tumor had been durably eradicated (Fig. 2A).

Because tumors are frequently diagnosed in humans when they have already reached a substantial size, we next investigated the efficacy of MK-4101 on large tumors (1,000 mm^3) by treating allografts ($n = 18$) with 80 mg/kg MK-4101 twice a day for 28 days. A robust 10-fold regression of the tumor masses was obtained in less than 15 days (Fig. 2B); however, after one-month treatment a slow relapse was observed.

Relapse was also described to occur during treatment of a preclinical model of medulloblastoma with vismodegib. Sequence analysis of relapsed tumors identified the D477G mutation in SMO. Interestingly this mutation is homologous to the D473H mutation identified in a medulloblastoma patient treated with vismodegib who relapsed after an initial response, suggesting that the preclinical model might have some predictive value with respect to resistance mechanisms. These data prompted us to investigate whether medulloblastomas that relapsed during MK-4101 treatment harbored mutations in SMO and particularly at position D477 (Supplementary Fig. S2). To this purpose, all 12 exons of the *Smo* gene in relapsed ($n = 14$) and untreated ($n = 4$) tumors collected during 3 different experiments were fully sequenced. Interestingly, we found no mutations in any exon, indicating that resistance to MK-4101 may be due to SMO-independent mechanisms.

We next set up a new experiment in which allografts (300 mm^3) were treated with 80 mg/kg of MK-4101 twice a day ($n = 10$) or with vehicle ($n = 10$) for a single day, before tumor explantation. MK-4101–treated tumors showed a significant decrease of 46.5% in weight compared with vehicle-treated tumors (average weight 0.145 vs. 0.27 g; $P = 0.002$; Fig. 2C), strongly suggesting cell death involvement in tumor shrinkage, confirmed by the significantly increased expression of active caspase in MK-4101- versus vehicle-treated tumors (0.06 ± 0.0095 vs. 0.006 ± 0.0097; $P < 0.0001$; Fig. 2D and E).

MK-4101 improves survival of *Ptch1*$^{+/-}$ mice

To further investigate the efficacy of MK-4101 we focused on primary medulloblastomas from neonatally irradiated Ptch1$^{+/-}$ mice, a highly penetrant model with 80% of mice developing full-blown medulloblastoma by 20 weeks of age (21). Quantification of tumor size in a subset of P1-irradiated *Ptch1*$^{+/-}$ mice ($n = 5$) of 8 weeks of age show an incidence of preneoplastic lesion of 80% (4/5) and an average size of 0.28 mm^2 (range 0.053–0.75 mm^2).

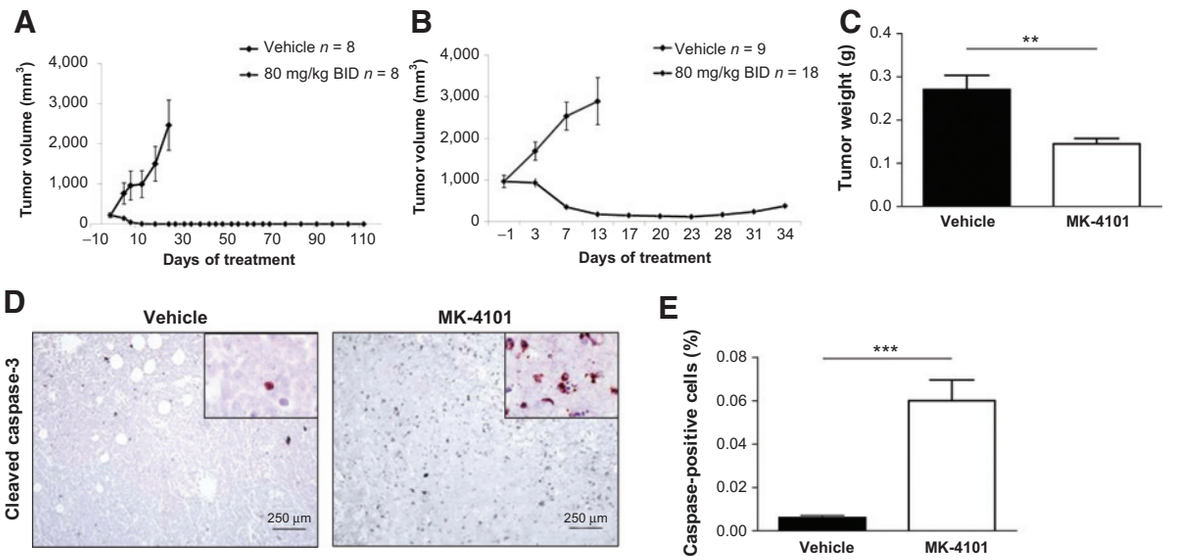

Figure 2.
Efficacy of MK-4101 on *Ptch1*$^{+/-}$ medulloblastoma allografts. A, durable tumor inhibition upon treatment of allografts (200 mm^3) with MK-4101 for 35 days. B, tumor regression in large medulloblastoma allografts (1,000 mm^3) treated with MK-4101 for 28 days. C, two doses of MK-4101 (80 mg/kg) significantly reduced of 46.5% tumor masses ($P = 0.002$). Immunohistochemical (IHC) analysis of cleaved caspase-3 in MK-4101- and vehicle-treated medulloblastoma (D) and relative quantification (E). A range of 8–10×10^3 cells were evaluated. BID, twice a day.

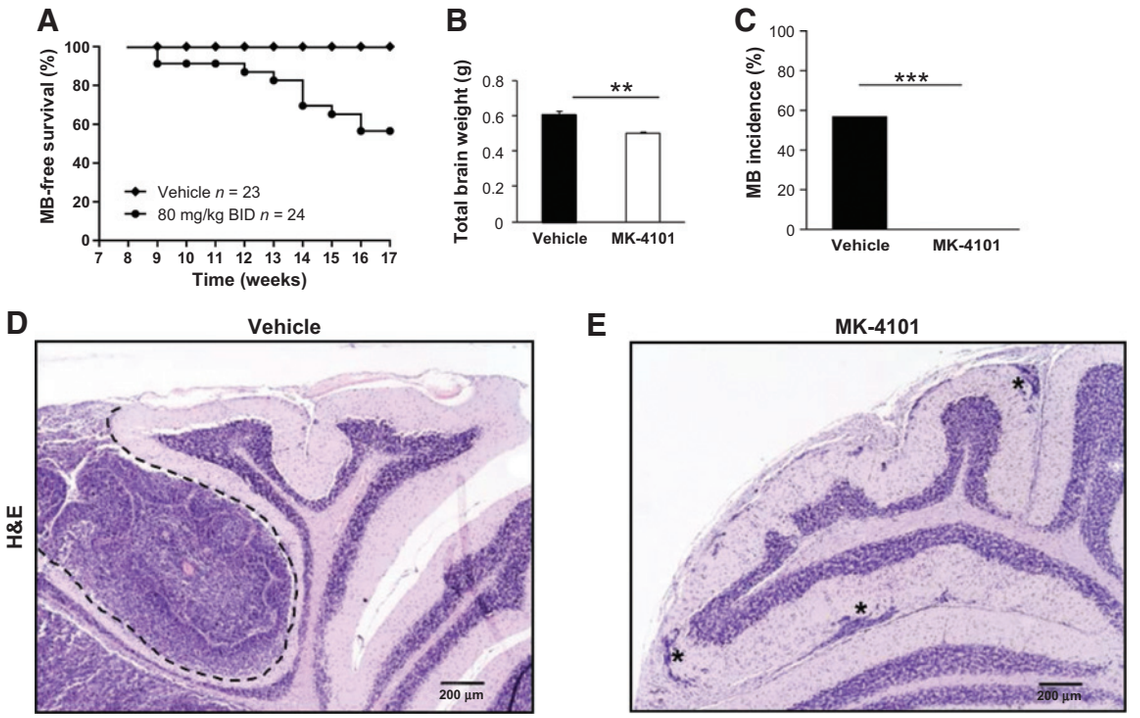

Figure 3.
Efficacy of MK-4101 on primary medulloblastomas in *Ptch1*$^{+/-}$ mice. A, treatment of *Ptch1*$^{+/-}$ mice with MK-4101 significantly increases mouse survival rates ($P = 0.0002$). B, an average weight decrease of 20% was detected in the brain of MK-4101- compared with vehicle-treated mice ($P = 0.0004$). C, medulloblastoma incidence showing complete lack of tumors in MK-4101–treated mice ($P < 0.0001$). D, histology of medulloblastoma (dashed line) in the brain of a vehicle-treated mouse. E, small foci of abortive tumor cells (*) on the cerebellum observed in 17% of MK-4101–treated animals. BID, twice a day.

We therefore asked whether treatment with MK-4101 (80 mg/kg twice a day) at this stage could prevent medulloblastoma formation and improve mouse survival. After 9 weeks of treatment, or earlier if clinical signs were observed, mice were euthanized, body and brain weights were determined, and brains were collected for histology. By the end of the treatment (17 weeks of age), none (0/24) of the MK-4101–treated mice had developed medulloblastoma-related lethargy, compared with over 50% (13/23) of the vehicle-treated mice (Fig. 3A), demonstrating that MK-4101 treatment significantly improved survival ($P = 0.0002$). A significant brain weight decrease of 17% was detected in MK-4101–treated animals as compared with vehicle-treated mice (0.501 vs. 0.604 g; $P = 0.0004$, Fig. 3B), reflecting the absence of tumor masses in the brains of MK-4101–treated animals. Moreover, highly significant differences in medulloblastoma incidence ($P < 0.0001$), between vehicle- (13/23) and MK-4101–treated mice (0/24), were revealed by histologic examination (Fig. 3C–E). Only four of MK-4101–treated mice (17%) presented small ectopic foci of abortive tumor cells on the cerebellar surface (Fig. 3E). Collectively, these data showed that treatment with MK-4101 efficaciously eliminates both early and more progressed medulloblastoma stages.

MK-4101 treatment inhibits BCC growth

BCC is one of the most common cancers in the western world. This tumor is locally aggressive and can present multiple recurrences. The skin of irradiated *Ptch1*$^{+/-}$ mice develops large infiltrative BCC-like tumors that faithfully recapitulate the etiology and histopathology of human BCC and closely resemble the genetics of the human counterpart in the complete loss of *Ptch1* (22, 29). We evaluated the ability of MK-4101 to act as therapeutic agent against BCC in this model. As a first step, because only 20% of irradiated *Ptch1*$^{+/-}$ mice develop grossly visible BCC, we explored the possibility to transplant BCC tumors as allografts. Two independent tumors with histologic features of BCC, including expression of cytokeratin-14, were transplanted giving rise to tumors that resembled donor tumors (Fig. 4A). Treatment of allografts ($n = 14$) with 80 mg/kg of MK-4101 twice a day for 4 weeks produced a dramatic inhibition of tumor growth of about 9-fold as compared with vehicle-treated allografts ($n = 14$; Fig. 4B), indicating that MK-4101 also efficiently suppresses BCC tumor growth.

MK-4101 reduces number and size of microscopic BCCs

Large infiltrative BCCs in irradiated *Ptch1*$^{+/-}$ mice develop through microscopically detectable preneoplastic stages, providing an ideal *in vivo* model to test chemotherapy or chemoprevention in BCC (22, 29). To test the effects of MK-4101 on early BCC stages, we established a group ($n = 23$) of *Ptch1*$^{+/-}$ mice irradiated as newborns. At 20 weeks of age, mice were randomly divided in two groups and treated with MK-4101 ($n = 12$; 80 mg/kg twice a day) or with vehicle only ($n = 11$). After 8 weeks of treatment, mice were euthanized and the shaved dorsal skin was processed for histologic examination. MK-4101 reduced the average number of microscopic BCCs per cm of skin surface length by about 33% compared with vehicle-

treated group (0.043 ± 0.020 vs. 0.064 ± 0.019; Fig 4C and D), although this difference did not reach statistical significance. Instead, MK-4101 significantly reduced by 34.8% the cross-sectional BCC area compared with vehicle-treated mice (1.44 ± 0.17 mm^2 vs. 2.21 ± 0.33 mm^2; $P < 0.05$; Fig. 4E). These results indicated that MK-4101 efficaciously reduced microscopic BCC tumor growth, supporting its effectiveness against tumor promotion/progression in the skin.

MK-4101 inhibits growth of grossly visible BCC in the skin of *Ptch1*$^{+/-}$-mutant mice

To analyze the potential of MK-4101 as therapeutic treatment against primary BCCs, thirteen tumor-bearing mice were randomly divided in two groups, treated with MK-4101 (80 mg/kg twice a day; $n = 6$) or vehicle ($n = 7$) for about 4 weeks. During this interval, the tumor size showed a 3-fold increase in vehicle-treated mice, while it remained substantially unchanged in MK-4101–treated mice (Fig. 4F), indicating that MK-4101 strongly inhibits BCC growth *in vivo*.

MK-4101 treatment of BCC inhibits the Hh pathway and induces antiproliferative and proapoptotic responses

The ability of MK-4101 to suppress Hh pathway activity in BCC was investigated by comparing *Gli1* mRNA expression levels in BCC before and after treatment with 80 mg/kg of MK-4101. Pre- and postdose biopsies at 6 ($n = 3$) and 12 hours ($n = 3$) were assayed for *Gli1* expression. Compared with the predose biopsy, tumors treated with MK-4101 show a progressive reduction in *Gli1* expression 6 and 12 hours postdose (Fig 4G). We also tested the expression of proliferative and apoptotic markers in pre- and postdose biopsies at 6 ($n = 1$) and at 12 hours ($n = 4$). Compared with the predose biopsy, a significant decrease ($P = 0.024$) in the fraction of Ki-67–positive cells was found in the tumor 6 hours after treatment with MK-4101 (Fig 4H and I). A trend towards decreased proliferation was also detected 12 hours postdose, although this difference did not reach statistical significance (Fig. 4I). Quantification of the fraction of cleaved caspase-3–positive cells shows a small increase of 50% at 6 hours ($P = 0.73$) and a dramatic 40-fold increase at 12 hours (predose biopsies: 0.06875 ± 0.0195 vs. postdose biopsies: 2.79 ± 0.8613; $P = 0.0045$; Fig. 4J and K). Altogether, these results provide clear evidence that treatment with MK-4101 effectively reduces the growth potential of BCCs and elicits a strong apoptotic response.

Gene expression profiling of MK-4101 treatment in medulloblastoma

The strong antitumor effect of MK-4101 led us to investigate its molecular mechanisms by addressing the modification of gene expression profiles in medulloblastoma elicited by MK-4101 using microarray analysis. Animals were randomized into groups ($n = 6$ per group) and tumor samples explanted at several time points following 40 or 80 mg/kg of MK-4101 once a day (1, 6, 12, 24, and 36 hours), twice a day (24 and 36 hours) or vehicle treatment (Fig. 5A).

Although a clear trend for higher deregulation at 80 mg/kg was apparent from the individual gene expression values, for example, for *Gli1*, no significant differential gene expression was detected between time-matched datasets at 40 and 80 mg/kg once a day (q value cutoff 0.02; Fig. 5D; Supplementary Table S2). Data from the 40 and 80 mg/kg groups was therefore pooled and compared with the time-matched untreated control samples.

Upon MK-4101 once a day treatment, changes in gene expression were detected starting at 6 hours (Fig. 5B and C). These changes increased at 12 and 24 hours postdose and disappeared at 36 hours. Instead, after MK-4101 twice a day treatment, changes in gene expression were maintained up to 36 hours (Fig. 5C).

We next performed a gene-set enrichment analysis (30, 31) against canonical pathways on the list of genes emerging from the analysis, separately for each time point. Downregulation of the Hh pathway dominates the signature at 6 hours, intensifies at 12 hours, starts to decline at 24 hours in once a day samples and attenuates from 24 to 36 hours in the twice a day treated samples, with *Gli1* showing the strongest downregulation (up to 17-fold at 12 hours; Fig 5D). Moreover, a considerable number of genes deregulated by MK-4101 belong to the DNA replication and cell-cycle control pathways. Among the first genes to be deregulated at 6 hours and, later on, at 12 and 24 hours, many are related to the G_1-S transition, like *cyclin D1* and *CDK6*, followed by *cyclin E1* and *CDK2*, several *E2F* variants (1–3, 7, 8), *cdc6*, and *cdc25a*. In samples taken at later time points (see twice a day samples at 36 hours) induced changes were instead focused on regulators of later cell-cycle checkpoints such as *cyclins A* and *B*. The most downregulated gene at 24 hours following once a day (17-fold) and twice a day treatment (15-fold) was *Wnt inhibitory factor* (*WIF1*; Supplementary Table S2), also known to modulate the diffusion of lipid-modified Hh (32). Instead, the most upregulated gene (up to about 5.6-fold) at 6, 12, and 24 hours once a day was *IGFBP5* (Supplementary Table S2). Interestingly, this gene is responsive to Hh (33), and it appears implicated in growth arrest and apoptosis in several tissues (34–36). Altogether, the microarray data indicate that MK-4101 targets the Hh pathway and induces cell-cycle deregulation and a block of DNA replication.

MK-4101 arrests cells in G_1 and G_2 phases

To further dissect the mechanism of tumor growth inhibition by MK-4101 and confirm microarray data, medulloblastoma and BCC single-cell suspensions were treated with a saturating dose MK-4101 (10 μmol/L) to maximize effects. Cell cycle was analyzed by FACS monitoring EdU incorporation. Medulloblastoma cells treated with MK-4101 for 60 hours showed cell-cycle arrest with a nearly complete disappearance of the S-phase subpopulation, a prominent increase of the G_1 population and, to a minor extent, of the G_2 population, indicative of a cell-cycle block in these two phases (Fig. 6A). Moreover, an increase in the sub-G_1 population was observed, indicative of underlying cell death. BCC cells treated with MK-4101 for 72 hours showed similar, although less pronounced effect (Fig. 6B), probably due to the lower growth rate of BCC compared with medulloblastoma cells. The cell-cycle blocks in G_1–S and G_2–M phases were confirmed by a remarkable decrease in cyclin D1 protein and accumulation of cyclin B1 protein, detected by Western blot analysis after MK-4101 treatment both in medulloblastoma and BCC tumor cells (Fig. 6C and D). Altogether, these results confirmed that MK-4101 inhibits medulloblastoma and BCC tumor growth by arresting cell cycle and inducing apoptosis.

Discussion

The Hh pathway is a key oncogenic pathway and mutations in its components drive the formation of medulloblastoma and BCC in

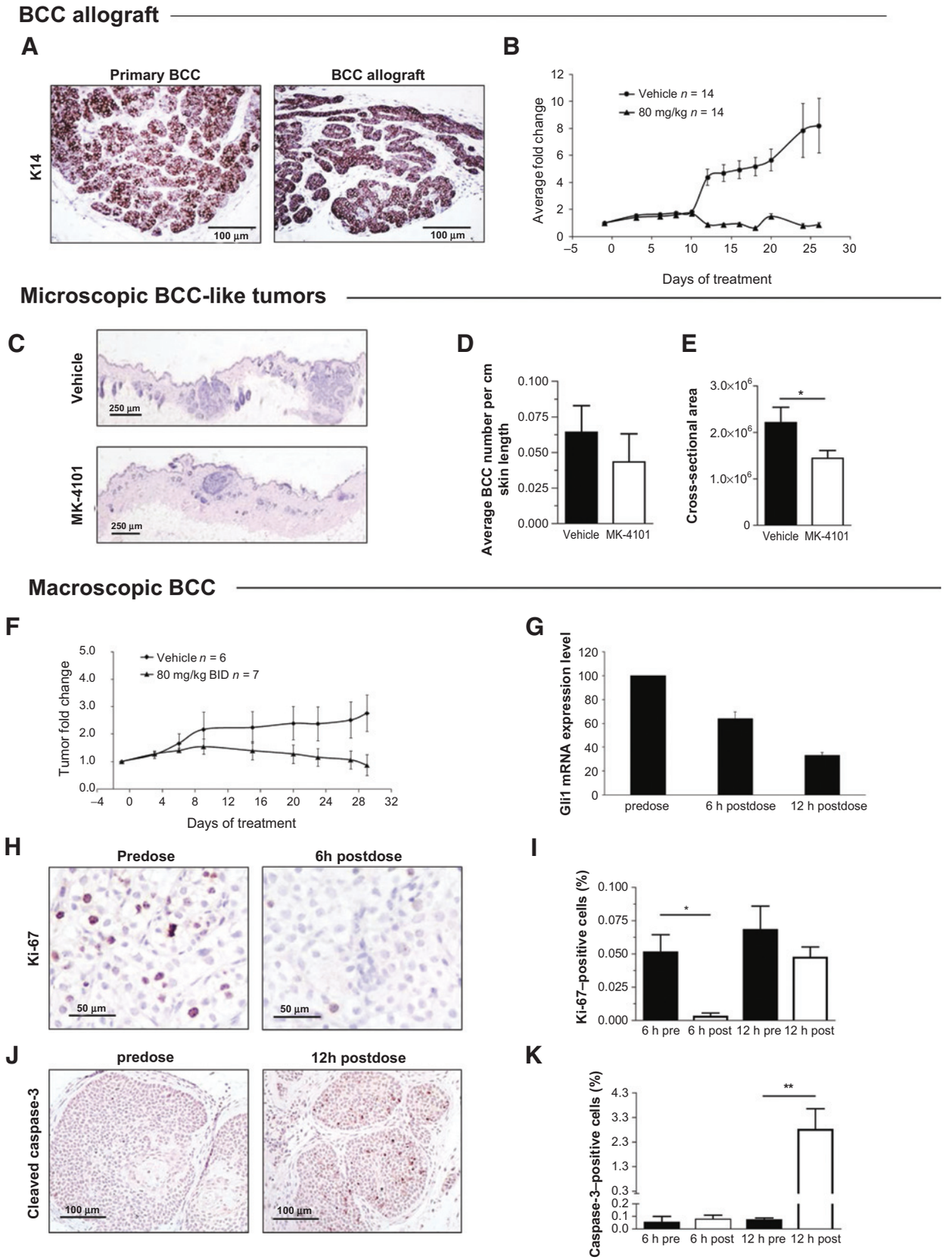
BCC allograft
A
Primary BCC
BCC allograft
K14
100 μm
100 μm
B
Vehicle n = 14
80 mg/kg n = 14
Average fold change
Days of treatment
Microscopic BCC-like tumors
C
Vehicle
MK-4101
250 μm
250 μm
D
Average BCC number per cm skin length
Vehicle
MK-4101
E
Cross-sectional area
Vehicle
MK-4101
Macroscopic BCC
F
Vehicle n = 6
80 mg/kg BID n = 7
Tumor fold change
Days of treatment
G
Gli1 mRNA expression level
predose
6 h postdose
12 h postdose
H
Predose
6h postdose
Ki-67
50 μm
50 μm
I
Ki-67–positive cells (%)
6 h pre
6 h post
12 h pre
12 h post
J
predose
12h postdose
Cleaved caspase-3
100 μm
100 μm
K
Caspase-3–positive cells (%)
6 h pre
6 h post
12 h pre
12 h post

mice and humans. However, recent evidence showing the involvement of this pathway in a larger number of cancers in which the pathway relies on paracrine activation (37), without the need of mutational inactivation, is stimulating research strategies to develop new Hh pathway inhibitors for pharmacologic intervention. Although no physiologic SMO inhibitors have been identified so far, efforts to inhibit Hh pathway have been focused on this protein, considered the most druggable target of the pathway (38).

We focused on MK-4101, a novel SMO antagonist, that is structurally dissimilar from other marketed SMO antagonists in clinical development. MK-4101 showed excellent drug-like properties, was brain-permeable, and potentially active on clinically relevant SMO mutants. In this study, we show that MK-4101 is capable of eliminating BCC and medulloblastoma tumors developing in *Ptch1*$^{+/-}$ mice, a model that recapitulates all the salient features of the corresponding human tumors. Of note, beside antitumor response in transplanted tumors, MK-4101 was highly active against medulloblastoma and BCC arising at their primary location in the mouse cerebellum and skin, which could be more predictive of its clinical efficacy. Interestingly, MK-4101 preclinical antitumor efficacy and pharmacokinetic/pharmacodynamic profile were comparable with those of vismodegib.

The efficacy of MK-4101 against initial medulloblastoma stages in the cerebellum of tumor-initiated *Ptch1*$^{+/-}$ mice underlines the capability of MK-4101 to cross a still intact blood–brain barrier. In addition, we report a robust response of MK-4101 in the skin of *Ptch1*$^{+/-}$ mice, in which this compound significantly inhibited the growth of microscopic and full-blown BCC. Altogether, these results suggest MK-4101 as an appealing candidate for treatment of Hh-driven tumors of the brain and skin.

Our tumor profiling data showed that a single MK-4101 dose decreases the expression level of Hh pathway target genes including *Gli1*, *Gli2*, *Ptch1*, *Ptch2*, and *HHip*, with *Gli1* being the most sensitive marker. The maximum decrease in Hh pathway expression was observed at 6–12 hours postdose and lasted 24 hours, demonstrating the ability of this orally administrable compound to inhibit the Hh pathway. Importantly, no obvious side effects were observed during treatment, indicating that MK-4101 is well tolerated in adult mice.

Linked to the extreme sensitivity of medulloblastoma and BCC to MK-4101, capable of inducing dramatic tumor regression with a few treatments, we detected in both tumors postdose a robust decrease in cell proliferation and a marked induction of apoptosis, leading to rapid tumor shrinkage. Analogous rapid responses of medulloblastoma and BCC to treatment with vismodegib were reported in clinical trials (39). However, the appearance of drug -resistant tumors after an initially rapid response to vismodegib in a patient with metastatic medulloblastoma, underscored the need for alternative drugs against SMO or other pathway components (18, 27), and in fact, several preclinical studies have begun using combinations of SMO inhibitors with PI3K/mTOR inhibitors or arsenic trioxide and itraconazole (40–42). For MK-4101, although no relapse was observed for 9–12 weeks after treatment of small size allografts (150–200 mm^3) or primary tumors in *Ptch1*$^{+/-}$ mice, we occasionally observed relapse in large tumors, suggesting that secondary resistance might occur, even though it is not a general phenomenon. To address the mechanism of resistance to MK-4101, we sequenced the full *Smo* gene in relapsed mouse medulloblastomas and did not find mutations. This lack of mutations in *Smo*, together with the modest loss of potency of MK-4101 on vismodegib-resistant D477G mutant are strongly suggestive of a different binding mode and possibly of a different spectrum of clinical activity of MK-4101, compared with vismodegib. However, the mechanism of resistance of MK-4101 will deserve further investigations.

In this study, we show that *Gli1* expression, the most sensitive marker of Hh pathway activity, is strongly inhibited by MK-4101, both in medulloblastoma and BCC tumors. Mechanistically, cDNA microarray analysis of gene expression profiles in response to MK-4101 revealed a strong downregulation of genes involved in cell-cycle control, such as those regulating cell-cycle progression at G_1–S, including *E2F2*, *cyclin D1 (CCND1)*, *cyclin E2 (CCNE2)*, and *CDK2*. Consistently, flow cytometric data demonstrated cell-cycle arrest in G_1 and, to a minor extent, in G_2–M phases in response to MK-4101. The blockade of cells at G_1–S and G_2–M was also evidenced by cyclin D1 degradation and cyclin B1 accumulation detected by Western blot analysis after MK-4101 treatment in both medulloblastoma and BCC tumor cells. Altogether, our data indicate that the antitumor mechanism of MK-4101 in Hh-driven cancer involved genes regulating DNA replication, cell-cycle progression, and proliferation.

Interestingly, *IGFBP5* was among the most highly upregulated genes by MK-4101. IGFBP5 has been shown to inhibit Hh-induced proliferation in neural precursors of the developing cerebellum and to be involved in apoptosis in the brain following hypoxic–ischemic injury (34, 35). In addition, consistent with the notion that Hh may act as a negative-feedback regulator of Wnt signaling in several settings (43–45), the *Wnt inhibitory factor (WIF)* was markedly downregulated in response to MK-4101-dependent inhibition of Hh pathway. These findings suggest that interplay among Hh, IGF, and Wnt signaling pathways might be pivotal in Hh-dependent tumorigenesis. Exploitation of these interactions may also have deep implications for the design of combinatorial molecularly targeted anticancer therapies.

In summary, although many SMO inhibitors have been identified and are currently in drug development, several

Figure 4.

Efficacy of MK-4101 on BCC allografts and primary BCC-like tumors in *Ptch1*$^{+/-}$ mice. A, BCC allograft resembling primary BCC both in morphology and cytokeratin-14 (K14) expression. B, growth inhibition of BCC allograft by MK-4101. C, decreased number and size of BCC precursor lesions in the skin of MK-4101- compared with vehicle-treated mice. D, average BCC number per cm of skin surface length, showing a decrease of 33% in MK-4101- compared with vehicle-treated mice. E, cross-sectional BCC area showing 34.8% reduction ($P < 0.05$) in the size of precursor lesions in MK-4101- compared with vehicle-treated mice. F, growth inhibition of primary BCC tumors by MK-4101. G, downregulation of *Gli* mRNA in MK-4101–treated primary BCC compared with predose tumor biopsy. Immunohistochemical analysis of Ki-67 (H) and quantification (I) showing a significant decrease in Ki-67 ($P < 0.05$) 6 hours after MK-4101 treatment compared with untreated tumors. Immunohistochemical analysis of cleaved caspase-3 (J) and quantification (K) showing a significant increase ($P = 0.0045$) 12 hours after MK-4101 treatment compared with untreated tumors. A minimum of 10^3 cells was examined for each time point. BID, twice a day.

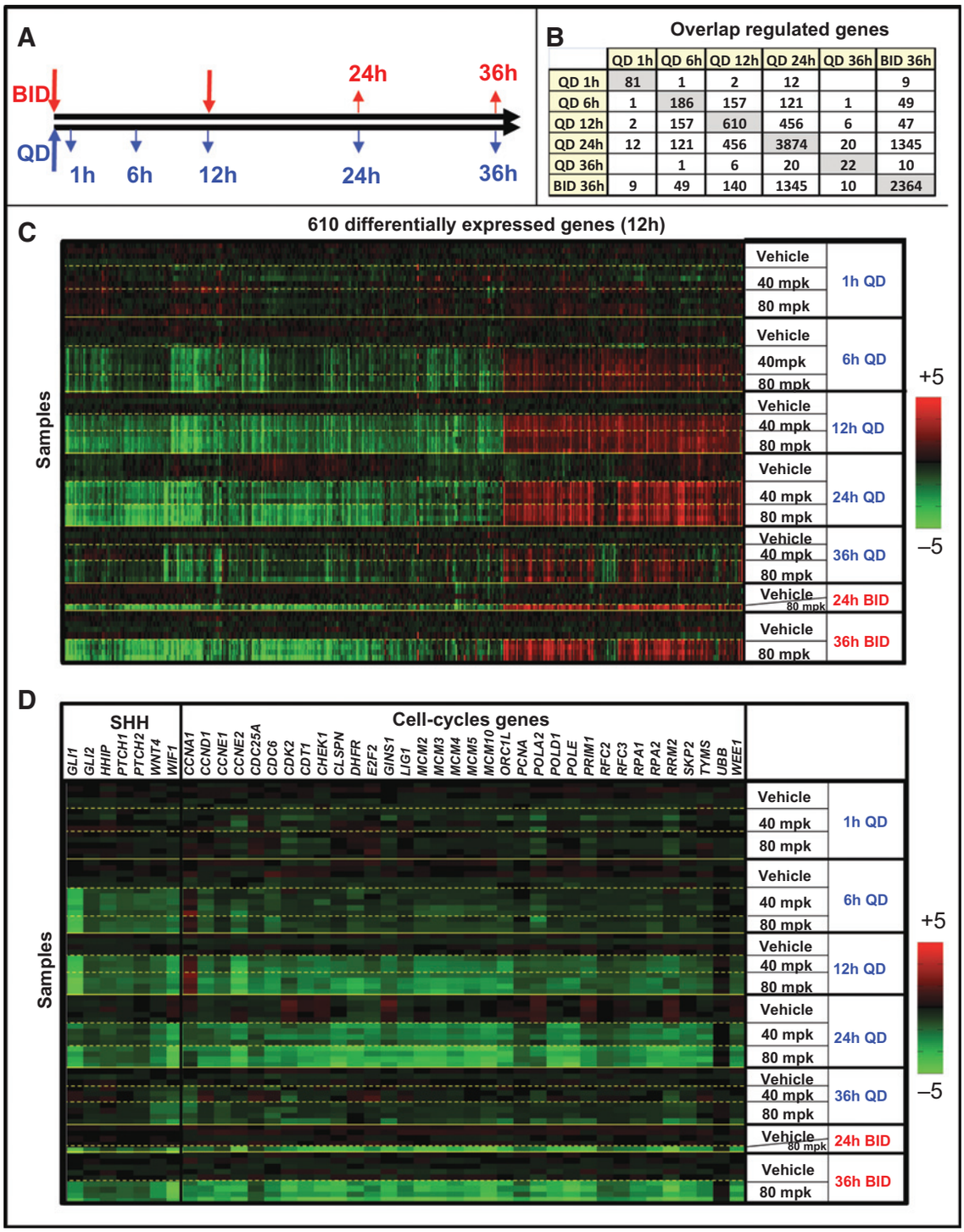

	QD 1h	QD 6h	QD 12h	QD 24h	QD 36h	BID 36h
QD 1h	81	1	2	12		9
QD 6h	1	186	157	121	1	49
QD 12h	2	157	610	456	6	47
QD 24h	12	121	456	3874	20	1345
QD 36h		1	6	20	22	10
BID 36h	9	49	140	1345	10	2364

Figure 5.
MK-4101–driven changes in tumor expression profiles. A, scheme of treatment and sample collection. B, overlap of genes differentially regulated in MK-4101- and vehicle-treated medulloblastoma as determined by the SAM algorithm. C, heatmap for 610 genes differentially regulated between 12 hours once a day (QD) treatment (40 and 80 mg/kg) and control group. D, changes induced by MK-4101 in genes from the Hh pathway (left) or cell-cycle–related genes (right). BID, twice a day.

features of MK-4101, such as strong antitumor activity, good blood–brain barrier penetration, lack of obvious side effects, as well as absence of acquired *Smo* mutations and potential activity on one of the major vismodegib-resistant mutants, makes this molecule an attractive drug candidate, combining excellent safety and efficacy.

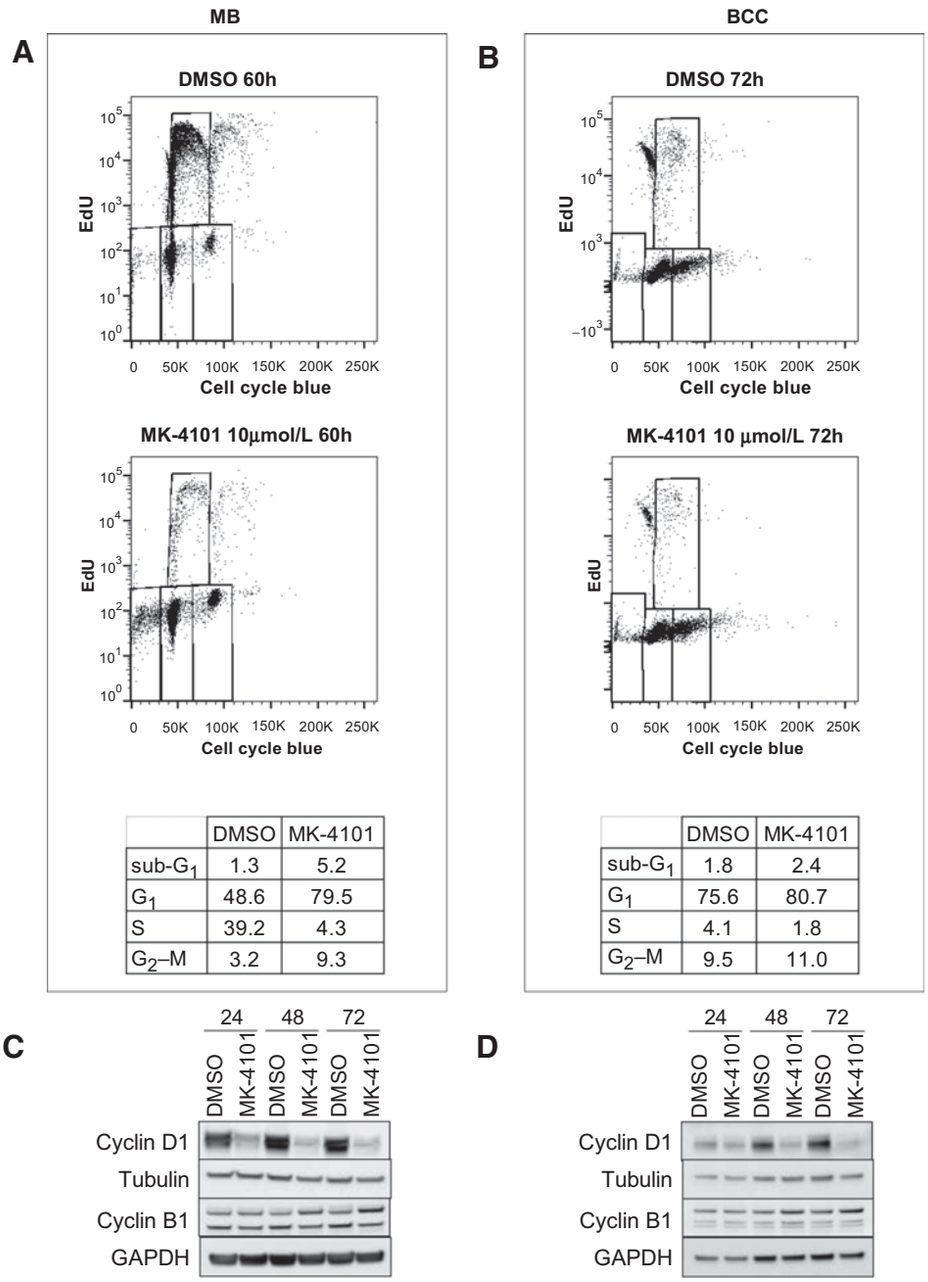

Figure 6.
Mechanism of growth inhibition by MK-4101 on medulloblastoma and BCC tumor cells. A and B, FACS analysis of medulloblastoma (A) or BCC (B) cells treated with MK-4101 for 60 or 72 hours, respectively, shows a block in both G_1 and G_2–M cell-cycle phases. C and D, Western blot analysis of cyclin D1, and B1 in medulloblastoma (C) and BCC (D) cells confirms cell-cycle arrest in both tumors.

Conclusions

Involvement of noncanonical Hh signaling in many cancers strongly encouraged the search for new inhibitors of this pathway with better safety and clinical efficacy. Results of this preclinical study show that MK-4101 impairs Hh oncogenic activity and induces a dose-dependent *Gli1* downregulation, as well as a significant tumor regression and improved survival *in vivo* via antiproliferative and proapoptotic responses. This strongly supports a potential role for this drug in the treatment of Hh-driven cancers. Further studies will be needed to explore the potential role of MK-4101 for the treatment of tumors dependent on noncanonical Hh signaling, and the use of MK-4101 in combinations of targeted therapies in medulloblastomas developing resistance to other SMO inhibitors.

Disclosure of Potential Conflicts of Interest

G. Filocamo was a Senior Research Biologist at Merck Sharp & Dohme. M. Brunetti was a technician at Merck Sharp & Dohme. F. Colaceci was a Senior Animal Technician at Merck Sharp & Dohme. R. Sasso was an Animal Technician at Merck Sharp & Dohme. A. Lahm was a Senior Research Fellow at Merck Sharp & Dohme. C. Steinkuhler is a former employee of Merck and has ownership interest (including patents) in Exiris. No potential conflicts of interest were disclosed by the other authors.

Authors' Contributions

Conception and design: G. Filocamo, C. Steinkuhler, S. Pazzaglia
Development of methodology: G. Filocamo, M. Brunetti, M. Tanori, E. Pasquali, M. Mancuso
Acquisition of data (provided animals, acquired and managed patients, provided facilities, etc.): M. Brunetti, F. Colaceci, R. Sasso, M. Tanori, E. Pasquali, R. Alfonsi, M. Mancuso, L. Di Marcotullio
Analysis and interpretation of data (e.g., statistical analysis, biostatistics, computational analysis): G. Filocamo, F. Colaceci, R. Sasso, M. Tanori, E. Pasquali, A. Lahm, C. Steinkuhler
Writing, review, and/or revision of the manuscript: G. Filocamo, A. Saran, C. Steinkuhler, S. Pazzaglia
Administrative, technical, or material support (i.e., reporting or organizing data, constructing databases): G. Filocamo, F. Colaceci, R. Sasso
Study supervision: G. Filocamo, S. Pazzaglia

Grant Support

This work was supported in part by Associazione Italiana Ricerca sul Cancro (AIRC): IGrant#15234 (to A. Saran) and IGrant#14723 (to L. D. Marcotullio).

The costs of publication of this article were defrayed in part by the payment of page charges. This article must therefore be hereby marked *advertisement* in accordance with 18 U.S.C. Section 1734 solely to indicate this fact.

Received May 6, 2015; revised February 22, 2016; accepted February 27, 2016; published OnlineFirst March 9, 2016.

References

1. Jiang J, Hui CC. Hedgehog signaling in development and cancer. Dev Cell 2008;15:801–12.
2. Hahn H, Wicking C, Zaphiropoulous PG, Gailani MR, Shanley S, Chidambaram A, et al. Mutations of the human homolog of Drosophila patched in the nevoid basal cell carcinoma syndrome. Cell 1996;85: 841–51.
3. Johnson RL, Rothman AL, Xie J, Goodrich LV, Bare JW, Bonifas JM, et al. Human homolog of patched, a candidate gene for the basal cell nevus syndrome. Science 1996;272:1668–71.
4. Gailani MR, Stahle-Backdahl M, Leffell DJ, Glynn M, Zaphiropoulos PG, Pressman C, et al. The role of the human homologue of Drosophila patched in sporadic basal cell carcinomas. Nat Genet 1996;14: 78–81.
5. Raffel C, Jenkins RB, Frederick L, Hebrink D, Alderete B, Fults DW, et al. Sporadic medulloblastomas contain PTCH mutations. Cancer Res 1997;57:842–5.
6. Xie J, Murone M, Luoh SM, Ryan A, Gu Q, Zhang C, et al. Activating Smoothened mutations in sporadic basal-cell carcinoma. Nature 1998; 391:90–2.
7. Dellovade T, Romer JT, Curran T, Rubin LL. The hedgehog pathway and neurological disorders. Annu Rev Neurosci 2006;29:539–63.
8. Rubin LL, de Sauvage FJ. Targeting the Hedgehog pathway in cancer. Nat Rev Drug Discov 2006;5:1026–33.
9. Lum L, Beachy PA. The Hedgehog response network: sensors, switches, and routers. Science 2004;304:1755–9.
10. Hahn H, Wojnowski L, Zimmer AM, Hall J, Miller G, Zimmer A. Rhabdomyosarcomas and radiation hypersensitivity in a mouse model of Gorlin syndrome. Nat Med 1998;4:619–22.
11. Aszterbaum M, Epstein J, Oro A, Douglas V, LeBoit PE, Scott MP, et al. Ultraviolet and ionizing radiation enhance the growth of BCCs and trichoblastomas in patched heterozygous knockout mice. Nat Med 1999;5: 1285–91.
12. Athar M, Li C, Tang X, Chi S, Zhang X, Kim AL, et al. Inhibition of smoothened signaling prevents ultraviolet B-induced basal cell carcinomas through regulation of Fas expression and apoptosis. Cancer Res 2004; 64:7545–52.
13. Romer JT, Kimura H, Magdaleno S, Sasai K, Fuller C, Baines H, et al. Suppression of the Shh pathway using a small molecule inhibitor eliminates medulloblastoma in Ptc1(+/−)p53(-/−) mice. Cancer Cell 2004; 6:229–40.
14. Gallinari P, Filocamo G, Jones P, Pazzaglia S, Steinkuhler C. Smoothened antagonists: a promising new class of antitumor agents. Expert Opin Drug Discov 2009;4:525–44.
15. Mas C, Ruiz i Altaba A. Small molecule modulation of HH-GLI signaling: current leads, trials and tribulations. Biochem Pharmacol 2010;80: 712–23.
16. Low JA, de Sauvage FJ. Clinical experience with Hedgehog pathway inhibitors. J Clin Oncol 2010;28:5321–6.
17. Von Hoff DD, LoRusso PM, Rudin CM, Reddy JC, Yauch RL, Tibes R, et al. Inhibition of the hedgehog pathway in advanced basal-cell carcinoma. N Engl J Med 2009;361:1164–72.
18. Rudin CM, Hann CL, Laterra J, Yauch RL, Callahan CA, Fu L, et al. Treatment of medulloblastoma with hedgehog pathway inhibitor GDC-0449. N Engl J Med 2009;361:1173–8.
19. Miller-Moslin K, Peukert S, Jain RK, McEwan MA, Karki R, Llamas L, et al. 1-amino-4-benzylphthalazines as orally bioavailable smoothened antagonists with antitumor activity. J Med Chem 2009;52:3954–68.
20. Skvara H, Kalthoff F, Meingassner JG, Wolff-Winiski B, Aschauer H, Kelleher JF, et al. Topical treatment of Basal cell carcinomas in nevoid Basal cell carcinoma syndrome with a smoothened inhibitor. J Invest Dermatol 2011;131:1735–44.
21. Pazzaglia S, Tanori M, Mancuso M, Rebessi S, Leonardi S, Di Majo V, et al. Linking DNA damage to medulloblastoma tumorigenesis in patched heterozygous knockout mice. Oncogene 2006;25:1165–73.
22. Mancuso M, Pazzaglia S, Tanori M, Hahn H, Merola P, Rebessi S, et al. Basal cell carcinoma and its development: insights from radiation-induced tumors in Ptch1-deficient mice. Cancer Res 2004;64:934–41.
23. Pazzaglia S, Mancuso M, Atkinson MJ, Tanori M, Rebessi S, Majo VD, et al. High incidence of medulloblastoma following X-ray-irradiation of newborn Ptc1 heterozygous mice. Oncogene 2002;21:7580–4.
24. Pazzaglia S, Tanori M, Mancuso M, Gessi M, Pasquali E, Leonardi S, et al. Two-hit model for progression of medulloblastoma preneoplasia in Patched heterozygous mice. Oncogene 2006;25:5575–80.
25. Balkovec JM, Thieringer R, Waddell S T, inventors; Merck Sharp & Dohme Corp., assignee. Triazole derivatives which are SMO antagonists. United States patent US 7691887 B2. 2010 Apr 6.
26. Atwood SX, Sarin KY, Whitson RJ, Li JR, Kim G, Rezaee M, et al. Smoothened variants explain the majority of drug resistance in basal cell carcinoma. Cancer Cell 2015;27:342–53.
27. Yauch RL, Dijkgraaf GJ, Alicke B, Januario T, Ahn CP, Holcomb T, et al. Smoothened mutation confers resistance to a Hedgehog pathway inhibitor in medulloblastoma. Science 2009;326:572–4.
28. Peukert S, He F, Dai M, Zhang R, Sun Y, Miller-Moslin K, et al. Discovery of NVP-LEQ506, a second-generation inhibitor of smoothened. ChemMedChem 2013;8:1261–5.
29. Pazzaglia S, Mancuso M, Tanori M, Atkinson MJ, Merola P, Rebessi S, et al. Modulation of patched-associated susceptibility to radiation induced tumorigenesis by genetic background. Cancer Res 2004;64:3798–806.
30. Subramanian A, Tamayo P, Mootha VK, Mukherjee S, Ebert BL, Gillette MA, et al. Gene set enrichment analysis: a knowledge-based approach for interpreting genome-wide expression profiles. Proc Natl Acad Sci U S A 2005;102:15545–50.
31. Mootha VK, Lindgren CM, Eriksson KF, Subramanian A, Sihag S, Lehar J, et al. PGC-1alpha-responsive genes involved in oxidative phosphorylation are coordinately downregulated in human diabetes. Nat Genet 2003;34: 267–73.
32. Han C, Lin X. Shifted from Wnt to Hedgehog signaling pathways. Mol Cell 2005;17:321–2.
33. Allan GJ, Zannoni A, McKinnell I, Otto WR, Holzenberger M, Flint DJ, et al. Major components of the insulin-like growth factor axis are expressed early in chicken embryogenesis, with IGF binding protein (IGFBP) -5 expression subject to regulation by Sonic Hedgehog. Anat Embryol 2003;207:73–84.
34. Fernandez C, Tatard VM, Bertrand N, Dahmane N. Differential modulation of Sonic-hedgehog-induced cerebellar granule cell precursor proliferation by the IGF signaling network. Dev Neurosci 2010;32:59–70.
35. Beilharz EJ, Klempt ND, Klempt M, Sirimanne E, Dragunow M, Gluckman PD. Differential expression of insulin-like growth factor binding proteins

(IGFBP) 4 and 5 mRNA in the rat brain after transient hypoxic-ischemic injury. Brain Res Mol Brain Res 1993;18:209–15.
36. Butt AJ, Dickson KA, McDougall F, Baxter RC. Insulin-like growth factor-binding protein-5 inhibits the growth of human breast cancer cells in vitro and in vivo. J Biol Chem 2003;278:29676–85.
37. Theunissen JW, de Sauvage FJ. Paracrine Hedgehog signaling in cancer. Cancer Res 2009;69:6007–10.
38. Onishi H, Katano M. Hedgehog signaling pathway as a therapeutic target in various types of cancer. Cancer Sci 2011;102:1756–60.
39. LoRusso PM, Rudin CM, Reddy JC, Tibes R, Weiss GJ, Borad MJ, et al. Phase I trial of hedgehog pathway inhibitor vismodegib (GDC-0449) in patients with refractory, locally advanced or metastatic solid tumors. Clin Cancer Res 2011;17:2502–11.
40. Buonamici S, Williams J, Morrissey M, Wang A, Guo R, Vattay A, et al. Interfering with resistance to smoothened antagonists by inhibition of the PI3K pathway in medulloblastoma. Sci Transl Med 2010;2:51ra70.
41. Kim J, Lee JJ, Gardner D, Beachy PA. Arsenic antagonizes the Hedgehog pathway by preventing ciliary accumulation and reducing stability of the Gli2 transcriptional effector. Proc Natl Acad Sci U S A 2010;107:13432–7.
42. Kim J, Aftab BT, Tang JY, Kim D, Lee AH, Rezaee M, et al. Itraconazole and arsenic trioxide inhibit Hedgehog pathway activation and tumor growth associated with acquired resistance to smoothened antagonists. Cancer Cell 2013;23:23–34.
43. Danesin C, Peres JN, Johansson M, Snowden V, Cording A, Papalopulu N, et al. Integration of telencephalic Wnt and hedgehog signaling center activities by Foxg1. Dev Cell 2009;16:576–87.
44. Ahn Y, Sanderson BW, Klein OD, Krumlauf R. Inhibition of Wnt signaling by Wise (Sostdc1) and negative feedback from Shh controls tooth number and patterning. Development 2010;137:3221–31.
45. Katoh Y, Katoh M. Hedgehog signaling pathway and gastrointestinal stem cell signaling network (review). Int J Mol Med 2006;18:1019–23.